IEEE Photonics Journal
An IEEE Photonics Society Publication

Open Access

Instantaneous Microwave Frequency Measurement Based on Two Cascaded Photonic Crystal Nanocavities

Volume 12, Number 6, December 2020

Li Liu
Wei Xue

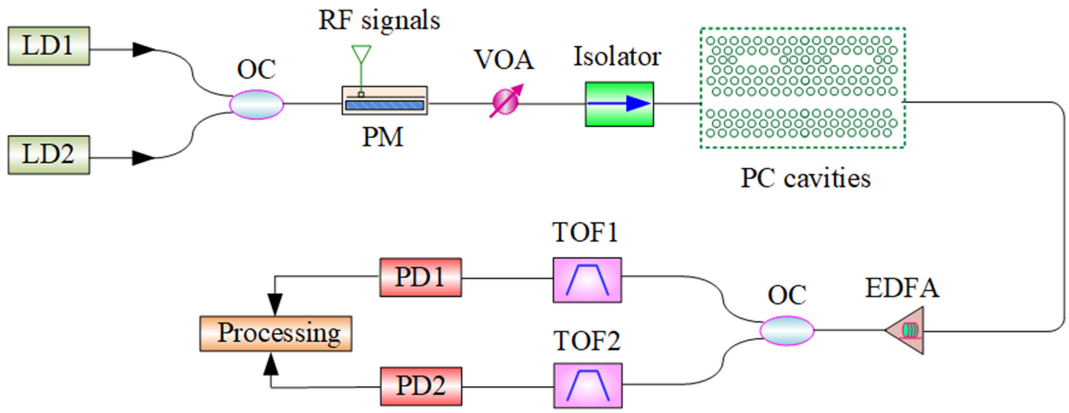

DOI: 10.1109/JPHOT.2020.3030256

IEEE photonics SOCIETY
IEEE

Instantaneous Microwave Frequency Measurement Based on Two Cascaded Photonic Crystal Nanocavities

Li Liu [1,2,3] **and Wei Xue** [1,2,3]

[1]School of Automation, China University of Geosciences, Wuhan 430074, China
[2]Hubei Key Laboratory of Advanced Control and Intelligent Automation for Complex Systems, Wuhan 430074, China
[3]Engineering Research Center of Intelligent Technology for Geo-Exploration, Ministry of Education, Wuhan 430074, China

DOI:10.1109/JPHOT.2020.3030256

Manuscript received June 30, 2020; revised October 5, 2020; accepted October 8, 2020. Date of publication October 13, 2020; date of current version October 21, 2020. This work was supported in part by the National Natural Science Foundation of China under Grant 61805215, and in part by the Wuhan Municipal Science and Technology Bureau under Grant 2019010701011410. Corresponding author: Li Liu (email: liliu@cug.edu.cn).

Abstract: We propose and experimentally demonstrate a photonic-assist measurement of microwave frequency by utilizing two cascaded photonic crystal (PC) cavities. By injecting different powers into the PC cavities, the device transmission spectra could be effectively manipulated. Consequently, the central frequencies of the microwave photonic filters (MPFs) can be flexibly adjusted. By utilizing the different MPF responses, adjustable amplitude comparison functions (ACFs) could be constructed. As the mapping relationships between the ACF ratios and the microwave frequencies are unique, the frequency with dynamic ranges could be measured according to the adjustable ACFs. The experimental results show that the measurement range of the microwave frequency is from 9 GHz to 19 GHz and the largest measurement errors are lower than 0.15 GHz. More importantly, the required optical power to manipulate the nanocavities is highly energy-efficient for on-chip nonlinear effect-based microwave measurements. The energy-efficient silicon device with compact size and low power is significant for dynamic frequency measurements in on-chip microwave systems.

Index Terms: Microwave frequency measurement, photonic crystal cavity, low power, low measurement error.

1. Introduction

In radio frequency (RF) systems, microwave frequency measurement is a fundamental function so as to transmit the RF signals to the specialized equipment and receivers [1]–[3]. Especially, photonic-assist approaches for microwave frequency measurements have attracted widespread attention due to its advantages of immunity to electromagnetic interference and large bandwidth [4]–[9]. In the past decades, numerous photonic methods for instantaneous microwave frequency measurements have been demonstrated based on optical fiber technology [10]–[12], which are unfavorable for large-scale on-chip integration. To realize better reliability and lower cost, silicon-on-insulator (SOI) technology provides a promising solution for on-chip optical signal processing [13]–[16]. One important theory is to build an amplitude comparison function (ACF). Subsequently,

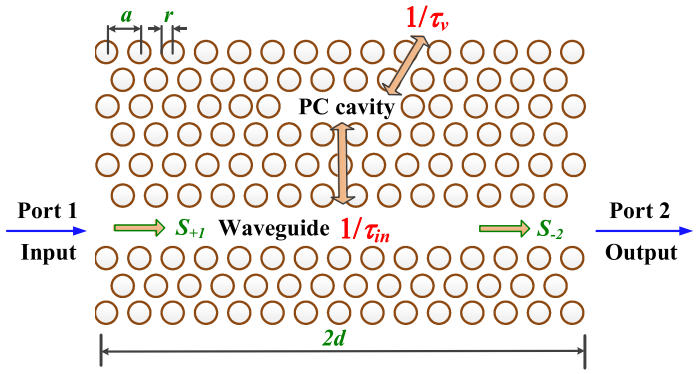

Fig. 1. Illustration of the photonic crystal nanocavity.

on the basis of the unique mapping relationship between the frequencies and power ratios in the function monotonic regions [17]–[21], the microwave frequency could be estimated. But the ACFs of many schemes are difficult to be flexibly adjustable, which could not meet the requirements of dynamic measurements and reconfigurable systems. Some important approaches have been proposed based on the tunable laser diodes [22] or multiple modulators [23]. Especially, nonlinear effects in integrated devices have been also utilized to realize adjustable ACFs, such as stimulated Brillouin scattering (SBS) [5] and Kerr nonlinearity [14]. Nevertheless, the relatively high powers of these schemes are not beneficial to build low-power microwave systems. Due to the above limitations, more compact devices with low-power mechanisms for photonic measurement of microwave frequency are highly desirable.

In this paper, a photonic-assisted scheme for microwave frequency measurement has been demonstrated by using energy-efficient cascaded photonic crystal (PC) cavities, whose size is as compact as 100 μm^2. With the measurement errors lower than 0.15 GHz, the microwave frequency ranges are larger than 10 GHz which could be further largely improved. Moreover, the measurement range could be flexibly adjusted with low power consumption, which is sufficient to be utilized in low-power dynamic microwave systems.

2. Operation Principle

The schematic image of the PC nanocavity is illustrated in Fig. 1, which includes a PC L3 nanocavity and a straight waveguide. The optical field injecting from port 1, the nanocavity optical mode and the optical signal outputting from port 2 are written as S_{+1}, u and S_{-2}, respectively. The symbols r, a and $2d$ represent the radii of the air holes, lattice constant and light propagation distance [24].

The relationships between u, light amplitudes S_{+1} and S_{-2} can be described as follows [24]

$$\frac{du}{dt} = \left(j\omega_0 - \frac{1}{\tau_{in}} - \frac{1}{\tau_v}\right)u + \sqrt{\frac{1}{\tau_{in}}}e^{-j\beta d}S_{+1} \tag{1}$$

$$S_{-2} = e^{-j2\beta d}\left(S_{+1} - \sqrt{\frac{1}{\tau_{in}}}e^{j\beta d}u\right) \tag{2}$$

$$\mathrm{T} = \left(\frac{S_{-2}}{S_{+1}}\right)^2 = \frac{(\omega-\omega_0)^2 + (\omega_0/2Q_v)^2}{(\omega-\omega_0)^2 + (\omega_0/2Q_v + \omega_0/2Q_{in})^2} \tag{3}$$

where the propagation constant is written as β and ω_0 is the cavity resonant angular frequency. The decay rates are described by $1/\tau_{in}$ (from the PC cavity into the waveguide) and $1/\tau_v$ (from

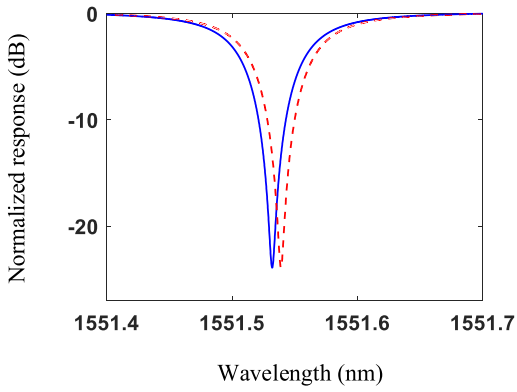

Fig. 2. Simulation of the nanocavity transmissions.

the PC cavity into the free space). The quality (Q) factors are expressed as Q_v ($Q_v = \tau_v\omega_0/2$) (the vertical Q) and Q_{in} ($Q_{in} = \tau_{in}\omega_0/2$) (the in-plane Q).

Owing to the cavity small mode volume and long resonant photon lifetime, the nonlinear effects (including Kerr effect, thermo-optic effect and plasma dispersion effect) in the PC nanocavity could be extremely enhanced. Therefore, the cavity transmission characteristics can be efficiently manipulated when injecting low input powers, which benefits for realizing energy-efficient signal processing devices.

Due to the nonlinear effects, the resonant frequency of the PC cavity could be denoted by

$$\omega' = \omega_0 + \Delta\omega_{\text{Kerr}} + \Delta\omega_{\text{thermal}} + \Delta\omega_{\text{plasma}} \tag{4}$$

where the resonant frequency shifts are written as $\Delta\omega_{\text{Kerr}}$ (induced by the Kerr effect), $\Delta\omega_{\text{thermal}}$ (thermo-optic effect) and $\Delta\omega_{\text{plasma}}$ (plasma dispersion effect). The thermal effect dominates the resonance shifts of the nanocavity. The detailed analysis of the cavity nonlinear effects could refer to ref. [25].

To theoretically research the transmission spectrum of the PC nanocavity, Fig. 2(a) shows the PC transmission spectra which are simulated by utilizing the above equations and the nonlinear coupled mode models [26]. The parameter τ_v and the cavity resonant wavelength are set to 0.6 ns and 1551.532 nm, respectively. Detailed physical parameters are given by ref. [27]. With injecting optical powers around -16 dBm and -25.9 dBm, the cavity transmission spectra are shown as the red dashed curve and the green solid curve, respectively. It is clear that the PC nanocavity could be tuned with high efficiency.

Figure 3(a) shows the operation principle of the photonic-assisted microwave frequency measurement is shown in Fig. 3(a). The laser diode 1 (LD1) and LD2 emit the optical carriers λ_1 and λ_2 respectively which are both injected into the phase modulator (PM). In the meantime, the PM is driven by a random RF signal to achieve optical double sideband (ODSB) signals. Then the ODSB signals are sent into the cascaded PC cavities. The original resonant wavelengths of the two nanocavities are λ_{c1} and λ_{c2}, shown as the green solid line in the dotted box. The optical carriers λ_1 and λ_2 are far away from the cavity resonances. The frequency intervals between the optical carriers λ_1 and the resonant peak λ_{c1}, λ_2 and λ_{c2} are f_1 and f_2, respectively. The output signals from the PC cavities are processed by the two tunable optical filters (TOFs) and photodetectors (PDs). Finally, Fig. 3(b) shows that two responses of the microwave photonic filters (MPFs) with central frequencies of f_1 (the blue line) and f_2 (the green line) could be obtained in the two PDs.

The obtained response in the PD could be represented by [28]

$$i_{AC}(f) \propto 4\pi^2 j P_0 J_0(\gamma) J_1(\gamma) H^*(f_s) H(f_s + f_{RF}) \tag{5}$$

where P_0 is the input power, J_0 and J_1 are the first-order and second-order Bessel functions, γ represents the phase modulation depth, f_{RF} and f_{s} are the RF signal frequency and optical carrier

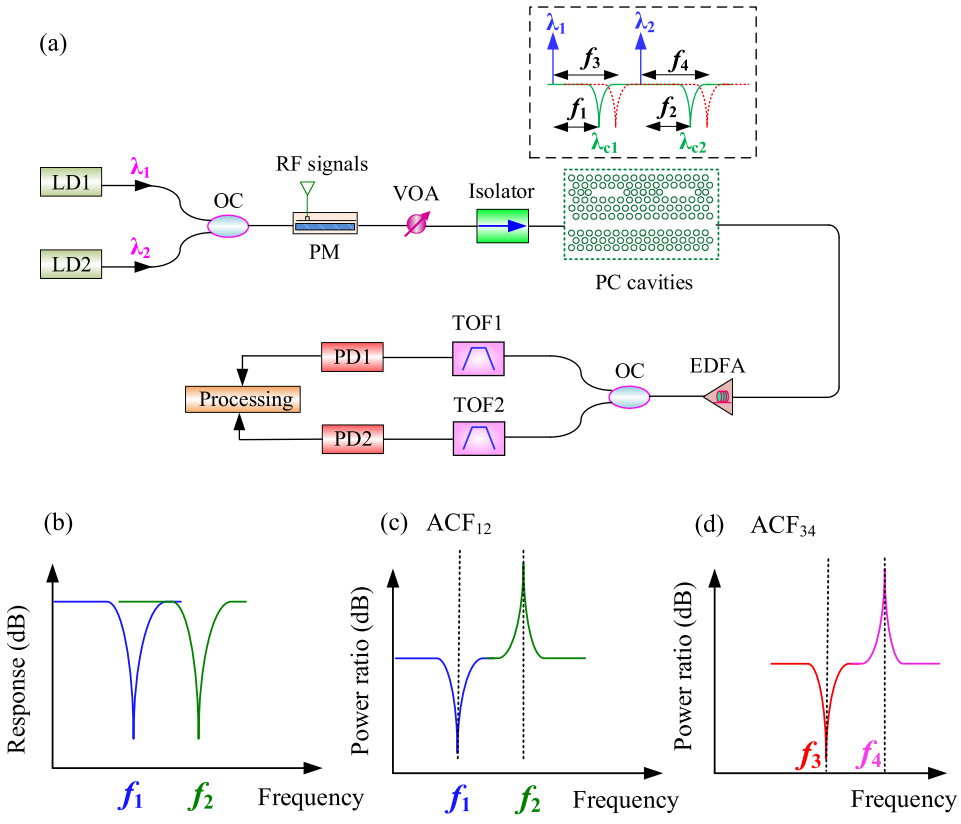

Fig. 3. (a) Illustration of the frequency measurement principle. (b) MPF responses. (c) ACF_{12}. (d) ACF_{34}.

frequency respectively, and $H(f)$ is the amplitude transmissions of the cavity [cavity 1: $H_1(f)$, cavity 2: $H_2(f)$].

The corresponding ACF_{12} can be denoted by

$$ACF12 = \frac{i_{AC}(f_1)}{i_{AC}(f_2)} = \frac{H_1{}^*(f_{s1})H_1(f_{s1}+f_{RF})}{H_2{}^*(f_{s2})H_2(f_{s2}+f_{RF})} \tag{6}$$

The measurement principle is described as follows. The two MPF responses (i_{AC1} and i_{AC2}) could be used to construct ACF_{12} ($ACF_{12} = i_{AC1}/\ i_{AC2}$), as shown in Fig. 3(c) and Eq. (6). In the monotonic increasing region of ACF_{12}, the microwave frequency and power ratio is a unique mapping relationship, thus the frequencies of the microwave signals could be estimated from f_1 to f_2. Subsequently, the control powers are injected into the cascaded PC cavities. Due to the cavity nonlinear effects, the device transmission spectra could be effectively shifted [the red dashed curve in the dotted box of Fig. 3(a)]. Consequently, the frequency intervals between λ_1 and the resonant wavelength of cavity 1, λ_2 and the resonance of cavity 2 are changed to f_3 and f_4, respectively. Thus the MPF frequencies can be accordingly tuned to f_3 and f_4. Therefore, Fig. 3(d) shows that the achieved ACF_{34} could be used to measure the microwave frequency from f_3 to f_4. Namely, the measurement range of the microwave frequency could be flexibly manipulated by adjusting the control powers.

To experimentally verify the measurement system of the RF frequency, we fabricated the cascaded PC L3 cavities on an SOI commercial wafer (the top silicon thickness: 220 nm). We utilized the E-beam lithography (EBL) to transfer the cavity layout to the photoresist and the inductively coupled plasma (ICP) to etch the upper silicon layer downward for 220 nm. The scanning electron

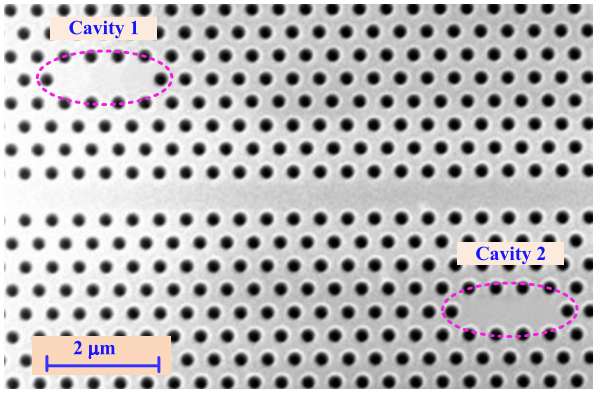

Fig. 4. The nanocavity SEM image.

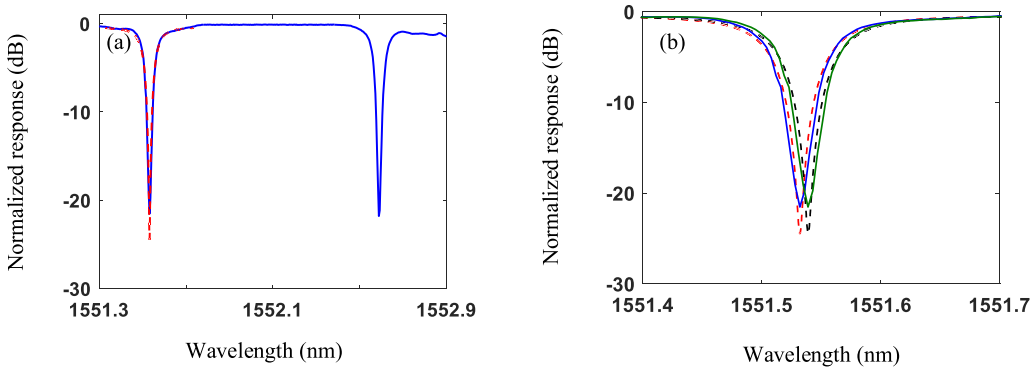

Fig. 5. (a) Measured transmission of the cascaded cavities. (b) The shifted transmissions of cavity 1.

microscope (SEM) image of the cascaded PC L3 cavities is shown in Fig. 4. The air hole radius and lattice constant of the cavity are 135 nm and 450 nm, respectively. The footprint of the whole device is 100 μm^2. The vertical grating couplers are used to couple the transverse-electric (TE) polarized light from the fiber to the silicon device. The coupling loss for a single side is 4 dB.

The measured transmission spectrum of the silicon cascaded nanocavities is shown as the blue line in Fig. 5(a). The resonant wavelengths of cavity 1 and cavity 2 are 1551.532 nm and 1552.59 nm, respectively. The extinction ratios are both higher than 20 dB. The Q factors of the two PC cavities are 2.28 $\times$ 10^4 and 2.16 $\times$ 10^4, respectively. The simulated transmission of cavity 1 is shown as the red dashed line, which is almost consistent with the measured response. The responses of the PC cavities are stable in a constant temperature environment, which could be realized by a temperature controller. To investigate the influence of the nonlinear effects on the cavity transmission characteristics, a control light with an optical power around -16 dBm (after subtracting the coupling loss) is utilized to manipulate the silicon cavity. Figure 5(b) illustrates the measured shifted transmission (the green solid curve) and the simulated transmission (the black dashed curve) of cavity 1. The measured results show that the tuning characteristics of the silicon nanocavities are energy-efficient.

3. Experimental Results

At first, the two optical carrier wavelengths λ_1 and λ_2 are fixed at 1551.46 nm and 1552.458 nm, which are 9 GHz and 16.5 GHz from the resonances of cavity 1 and cavity 2, respectively. The input microwave power is -5 dBm. Consequently, Fig. 6(a) illustrates that the frequencies of the obtained

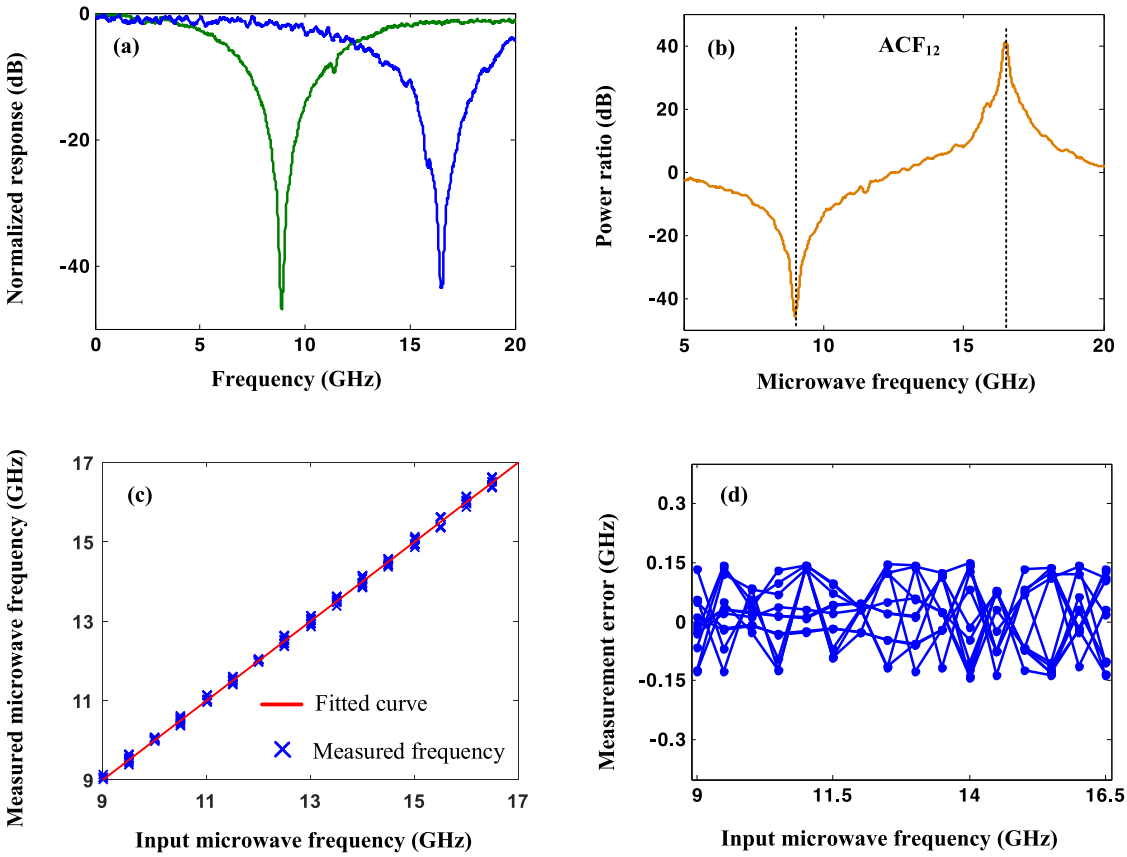

Fig. 6. (a) Two experimental MPF responses. (b) ACF_{12}. (c) The difference between the measured and input microwave frequencies. (d) Frequency errors.

microwave responses are 9 GHz (the green line) and 16.5 GHz (the blue line), respectively. The rejection ratios are about 47 dB and 44 dB, respectively. Subsequently, on the basis of the operation principle in Fig. 3, Fig. 6(b) shows that the two measured MPF responses are utilized to construct ACF_{12}. The frequency range and vertical height of the ACF monotonic increasing region are from 9 GHz to 16.5 GHz and 80 dB, respectively. Namely, the frequency resolution is about 10.67 dB/GHz, which could effectively identify the microwave frequency. Under multiple measurements, Fig. 6(c) shows the difference between the measured and input microwave frequencies ranging from 9 GHz to 16.5 GHz. As shown in Fig. 6(d), the most frequency measurement errors are around 0.1 GHz and the largest error is lower than 0.15 GHz.

Then, the device transmission spectrum is manipulated based on the nonlinear effects. With injecting optical power of -13.2 dBm, the two cavity resonances would be shifted to 1551.556 nm and 1552.61 nm, respectively. Consequently, the frequency intervals between λ_1 and the shifted resonant wavelength of cavity 1, λ_2 and the shifted resonance of cavity 2 change to 12 GHz and 19 GHz, respectively. Thus the central frequencies of the achieved another two MPF responses are 12 GHz and 19 GHz, shown as the green line and blue line in Fig. 7(a). Accordingly, Fig. 7(b) shows that a new ACF_{34} can be built through using the above microwave filters. The monotonic increasing region of ACF_{34} is from 12 GHz to 19 GHz with 86 dB vertical height. Namely, the frequency resolution is about 12.3 dB/GHz. With multiple measurement steps, Fig. 7(c) shows the difference between the measured and input microwave frequencies. Figure 7(d) illustrates that the largest frequency error is lower than 0.15 GHz. From Figs. 6 and 7, it can be seen that with maintaining the measurement errors lower than 0.15 GHz, the RF frequency can be investigated

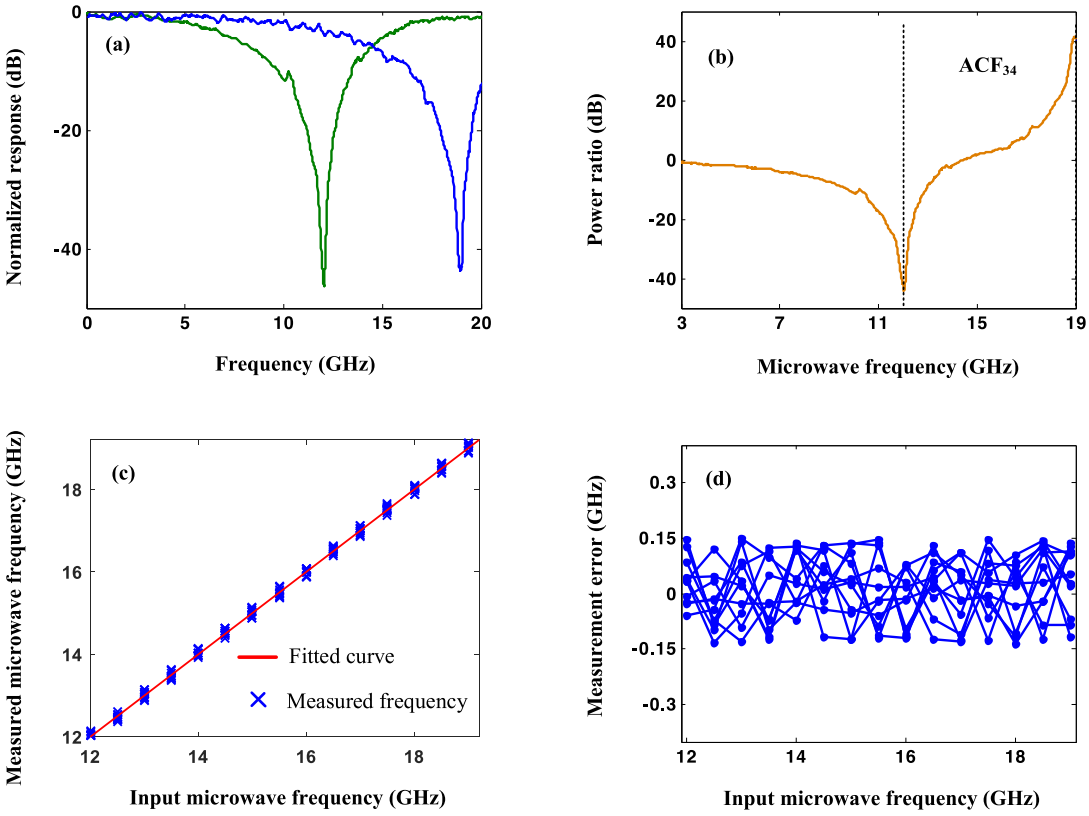

Fig. 7. (a) Another two microwave responses. (b) ACF_{34}. (c) The difference between the measured and input microwave frequencies. (d) Frequency errors.

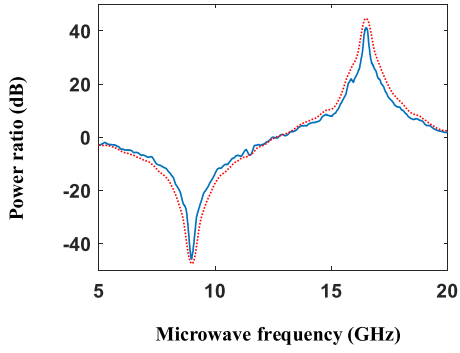

Fig. 8. The comparison between the measured ACF and the simulated ACF.

from 9 GHz to 19 GHz. Moreover, the measurement range could be flexibly adjusted with injecting a low power. Hence, the PC L3 cavities provide an energy-efficient solution for on-chip microwave measurements.

The theoretical responses of the PC cavity could be utilized to achieve the simulated ACF (the red dotted line), which is compared with the measured ACF (the blue solid line) in Fig. 8. The measurement errors are mainly attributed to the variation of the modulation characteristic and imperfect property of the silicon device. As we know, the modulation characteristic is related with the power of the input microwave signals. Consequently, RF drivers with precise amplification should

be used to equalize the RF power. The property of the silicon device (including the sidewall roughness) is determined by the fabrication technology. Better fabrication process and post-processing techniques could be used to improve the performance of the cavity. Meanwhile, by designing the PC cavities at the critical coupling, the cavity could achieve the highest extinction ratios. In this case, the MPF rejection ratios and ACF frequency resolutions can be accordingly increased, which are significant to improve the frequency measurement accuracy. Moreover, the required powers could be reduced. By adopting more advanced manufacturing methods and post-processing techniques [29]–[31], the device loss and Q factor can be largely improved [32]. On the other hand, the air hole positions of the PC cavity could be optimized to further increase the cavity Q factor and tuning efficiency [33]–[36]. Once the cavity Q factor is improved [37]–[41], the power consumption of the silicon device could be significantly reduced [42]–[45].

4. Conclusion

A photonic-assist scheme to measure the microwave frequency is experimentally demonstrated by using the silicon cascaded PC cavities. By using a low power to manipulate the cavities, the RF frequency can be characterized from 9 GHz to 19 GHz with flexibly adjustable ranges and 0.15 GHz measurement errors. There are three major advantages of the proposed scheme. Firstly, the proposed approach demonstrates microwave frequency measurements with flexibly adjustable measurement ranges based on the nonlinear effects in nano-cavities, which could avoid the requirement of tunable laser diodes. Secondly, the required power consumption to drive the integrated devices of other nonlinear effect-based schemes are 20 dBm [9], 18.7 dBm [14] and -3.9 dBm [18], respectively. Thirdly, the device sizes of the above schemes are 6.5 cm long [9] and 35 cm long [14]. In contrast, the power consumption and device size of the proposed method are as low as -13.2 dBm and 100 μm^2, respectively. Therefore, with various advantages of low-power consumption, adjustable measurement range, low errors and compact device size, the proposed approach is highly energy-efficient for dynamic microwave frequency measurements in radar and communication systems.

References

[1] S. Pan and J. Yao, "Photonics-based broadband microwave measurement," *J. Lightw. Technol.*, vol. 35, no. 16, pp. 3498–3513, Aug. 2017.

[2] S. Wang, G. Wu, Y. Sun, and J. Chen, "Photonic compressive receiver for multiple microwave frequency measurement," *Opt. Express*, vol. 27, no. 18, pp. 25364–25374, 2019.

[3] F. Zhou, H. Chen, X. Wang, L. Zhou, J. Dong, and X. Zhang, "Photonic multiple microwave frequency measurement based on frequency-to-time mapping," *IEEE Photon. J.*, vol. 10, no. 2, Apr. 2018, Art. no. 5500807.

[4] L. Liu, M. Ye, and Z. Yu, "Ultra-high peak rejection all-optical microwave filter based on the opto-mechanical effect," *IEEE Photon. Technol. Lett.*, vol. 32, no. 18, pp. 1155–1158, Sep. 2020.

[5] X. Long, W. Zou, and J. Chen, "Broadband instantaneous frequency measurement based on stimulated brillouin scattering," *Opt. Express*, vol. 25, no. 3, pp. 2206–2214, 2017.

[6] T. Hao, J. Tang, W. Li, N. Zhu, and M. Li, "Microwave photonics frequency-to-time mapping based on a Fourier domain mode locked optoelectronic oscillator," *Opt. Express*, vol. 26, no. 26, pp. 33582–33591, 2018.

[7] M. Burla, L. Cortés, M. Li, X. Wang, L. Chrostowski, and J. Azaña, "Integrated waveguide Bragg gratings for microwave photonics signal processing," *Opt. Express*, vol. 21, no. 21, pp. 25120–25147, 2013.

[8] B. Zhu, W. Zhang, S. Pan, and J. Yao, "High-sensitivity instantaneous microwave frequency measurement based on a silicon photonic integrated fano resonator," *J. Lightw. Technol.*, vol. 37, no. 11, pp. 2527–2533, Jun. 2019.

[9] H. Jiang *et al.*, "Wide-range, high-precision multiple microwave frequency measurement using a chip-based photonic brillouin filter," *Optica*, vol. 3, no. 1, pp. 30–34, 2016.

[10] X. Zou, B. Lu, W. Pan, L. Yan, A. Stöhr, and J. Yao, "Photonics for microwave measurements," *Laser Photon. Rev.*, vol. 10, no. 5, pp. 711–734, 2016.

[11] Z. Li, B. Yang, H. Chi, X. Zhang, S. Zheng, and X. Jin, "Photonic instantaneous measurement of microwave frequency using fiber Bragg grating," *Opt. Commun.*, vol. 283, no. 3, pp. 396–399, 2010.

[12] L. Bui *et al.*, "Instantaneous frequency measurement system using optical mixing in highly nonlinear fiber," *Opt. Express*, vol. 17, no. 25, pp. 22983–22991, 2009.

[13] L. Liu *et al.*, "Low-power all-optical microwave filter with tunable central frequency and bandwidth based on cascaded opto-mechanical microring resonators," *Opt. Express*, vol. 25, no. 15, pp. 17329–17342, 2017.

[14] M. Pagani *et al.*, "Low-error and broadband microwave frequency measurement in a silicon chip," *Optica*, vol. 2, no. 8, pp. 751–756, 2015.

[15] L. Liu, Y. Yang, Z. Li, X. Jin, W. Mo, and X. Liu, "Low power consumption and continuously tunable all-optical microwave filter based on an opto-mechanical microring resonator," *Opt. Express*, vol. 25, no. 2, pp. 960–971, 2017.
[16] L. Liu and X. Liu, "All-optical tunable microwave filter with ultra-high peak rejection and low-power consumption," *Opt. Express*, vol. 28, no. 9, pp. 13455–13465, 2020.
[17] M. Burla, X. Wang, M. Li, L. Chrostowski, and J. Azaña, "Wideband dynamic microwave frequency identification system using a low-power ultracompact silicon photonic chip," *Nat. Commun.*, vol. 7, 2016, Art. no. 13004.
[18] L. Liu, H. Qiu, Z. Chen, and Z. Yu, "Photonic measurement of microwave frequency with low-error based on an optomechanical microring resonator," *IEEE Photon. J.*, vol. 9, no. 6, Dec. 2017, Art. no. 5503511.
[19] X. Zou and J. Yao, "An optical approach to microwave frequency measurement with adjustable measurement range and resolution," *IEEE Photon. Technol. Lett.*, vol. 20, no. 23, pp. 1989–1991, Dec. 2008.
[20] W. Li, N. H. Zhu, and L. X. Wang, "Reconfigurable instantaneous frequency measurement system based on dual-parallel Mach-Zehnder modulator," *IEEE Photon. J.*, vol. 4, no. 2, 2012.
[21] D. Marpaung, "On-chip photonic-assisted instantaneous microwave frequency measurement system," *IEEE Photon. Technol. Lett.*, vol. 25, no. 9, pp. 837–840, May 2013.
[22] L. Liu, W. Xue, and J. Yue, "Photonic approach for microwave frequency measurement using a silicon microring resonator," *IEEE Photon. Technol. Lett.*, vol. 31, no. 2, pp. 153–156, Jan. 2019.
[23] N. Shi, Y. Gu, J. Hu, Z. Kang, X. Han, and M. Zhao, "Photonic approach to broadband instantaneous microwave frequency measurement with improved accuracy," *Opt. Commun.*, vol. 328, pp. 87–90, 2014.
[24] Y. Akahane, T. Asano, B. Song, and S. Noda, "Fine-tuned high-Q photonic-crystal nanocavity," *Opt. Express*, vol. 13, no. 4, pp. 1202–1214, 2005.
[25] L. Liu, S. Liao, W. Xue, and J. Yue, "Tunable all-optical microwave filter with high tuning efficiency," *Opt. Express*, vol. 28, no. 5, pp. 6918–6928, 2020.
[26] Y. Zhang *et al.*, "Low power and large modulation depth optical bistability in an si photonic crystal L3 cavity," *IEEE Photon. Technol. Lett.*, vol. 26, no. 23, pp. 2399–2402, Dec. 2014.
[27] X. Yang and C. W. Wong, "Coupled-mode theory for stimulated Raman scattering in high-Q/Vm silicon photonic band gap defect cavity lasers," *Opt. Express*, vol. 15, no. 8, pp. 4763–4780, Apr. 2007.
[28] Z. Tang, S. Pan, and J. Yao, "A high resolution optical vector network analyzer based on a wideband and wavelength tunable optical single-sideband modulator," *Opt. Express*, vol. 20, no. 6, pp. 6555–6560, 2012.
[29] C. Ocier, N. Krueger, W. Zhou, and P. Braun, "Tunable visibly transparent optics derived from porous silicon," *ACS Photon* , vol. 4, no. 4, pp. 909–914, 2017.
[30] L. Liu, T. Yang, and J. Dong, "Microwave photonic filter with a continuously tunable central frequency using an SOI high-Q microdisk resonator," *Chin. Phys. B*, vol. 23, no. 9, pp. 093201, 2014.
[31] K. Zang *et al.*, "Silicon single-photon avalanche diodes with nano-structured light trapping," *Nat. Commun.*, vol. 8, no. 1, pp. 628, 2017.
[32] L. Liu, J. Yue, X. Fan, and W. Xue, "On-chip passive optical diode with low-power consumption," *Opt. Express*, vol. 26, no. 25, pp. 33463–33472, 2018.
[33] M. Barth, J. Kouba, J. Stingl, B. Löchel, and O. Benson, "Modification of visible spontaneous emission with silicon nitride photonic crystal nanocavities," *Opt. Express*, vol. 15, no. 25, pp. 17231–17240, 2007.
[34] Y. Lai *et al.*, "Genetically designed L3 photonic crystal nanocavities with measured quality factor exceeding one million," *Appl. Phys. Lett.*, vol. 104, no. 24, 2014, Art. no. 241101.
[35] L. Liu and S. Liao, "Low-power active tunable microwave photonic filter using photonic crystal nanocavities," *IEEE Photon. Technol. Lett.*, vol. 32, no. 16, pp. 999–1002, Aug. 2020.
[36] S. Portalupi, M. Galli, M. Belotti, L. Andreani, T. Krauss, and L. O'Faolain, "Deliberate versus intrinsic disorder in photonic crystal nanocavities investigated by resonant light scattering," *Phys. Rev. B*, vol. 84, no. 4, 2011, Art. no. 045423.
[37] L. Liu, M. Ye, S. Liao, and W. Xue, "Silicon optical diode based on cascaded opto-mechanical microring resonators," *IEEE Photon. Technol. Lett.*, vol. 32, no. 15, pp. 952–955, Aug. 2020.
[38] S. A. Miller *et al.*, "Low-loss silicon platform for broadband mid-infrared photonics," *Optica*, vol. 4, no. 7, 2017, Art. no. 707.
[39] L. Liu, J. Dong, and X. Zhang, "Chip-integrated all-optical 4-bit gray code generation based on silicon microring resonators," *Opt. Express*, vol. 23, no. 16, pp. 21414–21423, 2015.
[40] E. A. Kittlaus, P. O. Weigel, and W. M. Jones, "Low-loss nonlinear optical isolators in silicon," *Nat. Photon.*, vol. 14, no. 6, pp. 338–339, 2020.
[41] M. Chen, L. Liu, L. Xu, M. Ye, X. Jin, and Z. Yu, "On-Chip all-optical tunable filter with high tuning efficiency," *IEEE Photon. J.*, vol. 12, no. 2, Apr. 2020, Art. no. 7800510.
[42] Y. Zhao, X. Wang, D. Gao, J. Dong, and X. Zhang, "On-chip programmable pulse processor employing cascaded MZI-MRR structure," *Front. Optoelectron.*, vol. 12, no. 2, pp. 148–156, 2019.
[43] L. Xu, L. Liu, M. Chen, and M. Ye, "All-silicon energy-efficient optical diode using opto-mechanical microring resonators," *IEEE Photon. J.*, vol. 12, no. 3, Jun. 2020, Art. no. 4501009.
[44] J. Gao, J. Sun, H. Zhou, J. Jiang, and Y. Zhou, "Design and fabrication of compact Ge-on-SOI coupling structure," *Front. Optoelectron.*, vol. 12, no. 3, pp. 276–285, 2019.
[45] Z. Chai, X. Hu, and Q. Gong, "Exciton polaritons based on planar dielectric si asymmetric nanogratings coupled with J-aggregated dyes film," *Front. Optoelectron.*, vol. 13, no. 1, pp. 4–11, 2019.